Electrohydrodynamically Induced Mixing and Pumping of Multifluid Systems in Microchannels

Radu CIMPEANU [1,*], Demetrios T. PAPAGEORGIOU [1]

* Corresponding author: Tel.: ++44 (0)2075 948369; Fax: ++44 (0)2075 948517; Email: radu.cimpeanu11@imperial.ac.uk
1: Department of Mathematics, Imperial College London, UK

Abstract We investigate electrostatically induced hydrodynamics in stratified flows. Vertical electric fields are used to destabilise stably stratified systems in channel geometries and generate interfacial motion. Efficient electrohydrodynamically actuated control processes are studied theoretically and shown to induce time dependent flows in small scale confined geometries without requiring an imposed velocity field or moving parts. Using linear stability theory, the most unstable wavenumbers for a given microscale geometry are identified in order to deduce electric field strengths that can be utilised to produce a required wave pattern. Starting from simple mechanisms, such as uniform field on-off protocols, promising results are presented in this context. Two-dimensional computations using the volume-of-fluid (VOF) method are conducted to fully validate the linear stability theory. Practical optimisation possibilities such as distributions of field strengths and time intervals between on and off positions are examined numerically in the nonlinear regime. We also propose a mechanism to induce pumping by generating a travelling wave voltage distribution on one or both of the electrodes. The generated flux allows for further improvement of the microfluidic mixing process and could have numerous other relevant ramifications. The analytical and numerical tools constructed enable the study of competitive alternatives in a broad spectrum of applications, from microfluidic mixing to electrostatically induced soft lithography.

Keywords: Microfluidics, Mixing, Induced Pumping, Control, Stability, Volume-of-Fluid Method

1. Introduction

Electrostatic control mechanisms underpin a wide range of modern industrial applications and are at the forefront of contemporary research. The impact of fluid interface manipulation has proven invaluable in the framework of production of increasingly smaller structural units, as well as the related context of efficient microfluidic mixing.

Recently, electrohydrodynamic stabilisation (or destabilisation) mechanisms have become increasingly popular. It has been shown (Cimpeanu et al., 2014) that horizontal electric fields can be used to suppress and control the Rayleigh-Taylor instability. Conversely, vertical electric fields (perpendicular to the fluid-fluid interface) can be used to generate interfacial dynamics in stably stratified systems, as presented in the seminal work of Melcher (1961) and Taylor and McEwan (1966).

Ozen et al. (El. Acta, 2006) have performed theoretical studies on the effects of an electric field on a flow of immiscible fluids in a channel. Long-wave stability analysis of the electrohydrodynamic stability of the interface between two superposed viscous fluids in a very general context has also been carried out (Ozen et al., 2007), with findings confirming the importance of exploiting electric field effects in small scale geometries.

One of the key aspects of the present work is the efficient use of electric fields in order to induce mixing in small scale geometries. Lee et al. (2011) provide a review of the most successful mixing devices pertaining to microfluidic flows. Passive mixing techniques usually exploit complicated spatial structures that elongate the path of an injected fluid and allow for enhanced molecular diffusion. Active mixers on the other hand do not require intricate patterns and exotic components; they involve the use of external forces, such as magnetism, electricity, time pulsing etc., with

convincing degrees of success.

The T-mixer is among the most popular active devices, as it provides a simple geometry and remarkable possibilities for expansion from the multi-physics perspective. Glasgow et al. (2003) and Goullet et al. (2005) have utilised sinusoidal time pulsing as a technique to force mixing. El Moctar et al. (2003) have shown drastic improvement in the mixing of an oil-oil configuration (different dyes) in a T-mixer under the action of electric fields.

We first present our mathematical model and governing equations in subsection 2.1, while subsection 2.2 is dedicated to the linear stability study of the problem. Having identified bands of unstable wavenumbers, we proceed and devise electric field protocols aimed at achieving efficient mixing (section 3) or inducing pumping (section 4) via electric field manipulation only. We use direct numerical simulations not only to validate the theoretical investigation, but also to conduct fully nonlinear studies that mimic experimental conditions and illustrate the effects of the suggested techniques. Finally, we formulate our conclusions in section 5.

2. Mathematical Model

We consider two immiscible, incompressible, viscous, perfect dielectric fluids of arbitrary constant densities, viscosities and permittivities, confined between parallel walls. The flow geometry is presented in the schematic in Fig. 1. The study is concentrated on horizontal channels with parallel walls aligned with the $x-$axis (in Cartesian coordinates), assumed to be sufficiently long, in line with experimental configurations in the literature. The channel walls are electrodes, such that an electric field of magnitude $\bar{V}^*/L$ is generated vertically, where L denotes the channel height (chosen lengthscale of the system) and $\bar{V}^*$ is the prescribed voltage potential difference across the channel. The interface between the two fluids is described by $y = S(x,t)$. We use subscripts 1 and 2 to denote relevant quantities in fluid 1 (bottom, defined by $-L/2 < y < S(x,t)$) and fluid 2 (top, defined by $S(x,t) < y < L/2$, respectively).

Fluid densities, viscosities and permittivities are written as $\rho_{1,2}, \mu_{1,2}$ and $\epsilon_{1,2}$, while velocity fields and pressures are represented by $\boldsymbol{u}_{1,2} = (u_{1,2}, v_{1,2})$ and $p_{1,2}$. To retain generality, we preserve gravitational effects via acceleration g and surface tension effects via the constant coefficient σ.

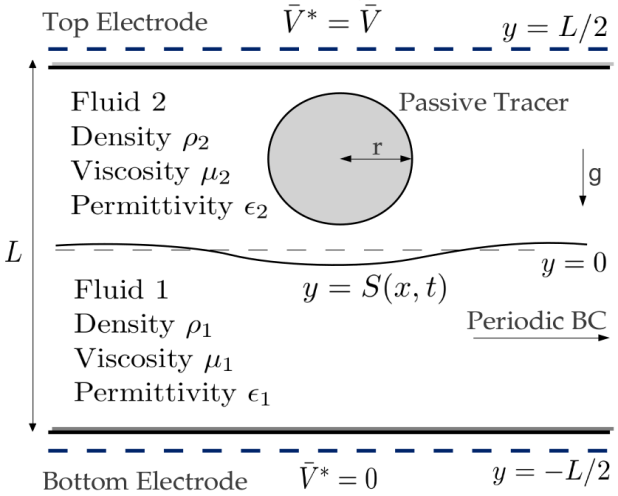

Fig. 1. Problem schematic.

2.1. Governing Equations

We first note that the fluids have constant electrical properties and there are no charges present in the flow, therefore hydrodynamic and electrostatic effects are coupled by nonlinear boundary conditions at the interface only. This translates into the following form for the momentum and continuity equations:

$$\rho_1(\boldsymbol{u}_{1t} + (\boldsymbol{u}_1 \cdot \nabla)\boldsymbol{u}_1) = \\ = -\nabla p_1 + \mu_1 \Delta \boldsymbol{u}_1 - \rho_1 g \boldsymbol{j}, \quad (1)$$

$$\rho_2(\boldsymbol{u}_{2t} + (\boldsymbol{u}_2 \cdot \nabla)\boldsymbol{u}_2) = \\ = -\nabla p_2 + \mu_2 \Delta \boldsymbol{u}_2 - \rho_2 g \boldsymbol{j}, \quad (2)$$

$$\nabla \cdot \boldsymbol{u}_{1,2} = 0. \quad (3)$$

Using the electrostatic approximation (see section 3 for further discussion), Maxwell's equations can be expressed as $\nabla \times \boldsymbol{E}_{1,2} = 0$ and $\nabla \cdot (\epsilon_{1,2}\boldsymbol{E}_{1,2}) = 0$, allowing us to define voltage potentials as $\boldsymbol{E}_{1,2} = -\nabla V_{1,2}$, in each of the fluids. The potentials satisfy Laplace's equation $(\partial/\partial x^2 + \partial/\partial y^2)V_{1,2} = 0$.

We define Dirichlet boundary conditions for bottom $V_1(x, -L/2, t) = 0$ and top $V_2(x, +L/2, t) = \bar{V}^*$ electrodes, producing the desired voltage potential difference.

At the sharp interface, $y = S(x,t)$, the

following conditions are imposed:

$$v_i = S_t + u_i S_x, \; i = 1,2, \tag{4}$$

$$[\boldsymbol{n}\cdot\boldsymbol{\mathcal{T}}\cdot\boldsymbol{n}]_2^1 = \sigma\cdot\kappa, \tag{5}$$

$$[\boldsymbol{t}\cdot\boldsymbol{\mathcal{T}}\cdot\boldsymbol{n}]_2^1 = 0, \tag{6}$$

$$[\boldsymbol{u}]_2^1 = 0, \tag{7}$$

$$[\boldsymbol{\varepsilon E}\cdot\boldsymbol{n}]_2^1 = 0, \tag{8}$$

$$[V]_2^1 = 0, \tag{9}$$

which are, in order of appearance, kinematic conditions, the normal stress balance, the tangential stress balance, continuity of velocities, voltage displacement field (Gauss's Law) and voltage. We use $[(\cdot)]_2^1 = (\cdot)_1 - (\cdot)_2$ to denote jumps across the interface, while the unit normal and tangent to the interface are defined as $\boldsymbol{n} = (-S_x, 1)/(1+S_x^2)^{1/2}$, $\boldsymbol{t} = (1, S_x)/(1+S_x^2)^{1/2}$ and $\kappa = S_{xx}/(1+S_x^2)^{3/2}$ is the expression for interfacial curvature. For the stress tensor in each of the regions 1 and 2, the reader is referred to Saville (1997). In our notation, the tensorial expression is

$$\boldsymbol{\mathcal{T}}_{mn} = -p\delta_{mn} + \mu\left(\frac{\partial u_m}{\partial x_n} + \frac{\partial u_n}{\partial x_m}\right) + \\ +\epsilon E_m E_n - \frac{1}{2}\epsilon|\boldsymbol{E}|^2\delta_{mn}. \tag{10}$$

We nondimensionalise by means of using a reference velocity U and reference lengthscale L, which translates to time being scaled by L/U and pressures by $\rho_1 U^2$. We use fluid 1 as reference and introduce the following dimensionless parameters:

$$\tilde{\mu} = \mu_1/\rho_1 UL, \; \tilde{\sigma} = \sigma/\rho_1 g L^2, \\ \tilde{g} = gL/U^2, \quad V^* = UL\sqrt{\rho_1/\epsilon_0}, \tag{11}$$

corresponding to an inverse Reynolds number (dimensionless viscosity), an inverse Weber number, an inverse square Froude number and a voltage scaling. The permittivity of free space is denoted as ϵ_0. We also define relevant ratios in the model as

$$r = \rho_1/\rho_2, \; m = \mu_2/\mu_1, \; \epsilon = \epsilon_1/\epsilon_2. \tag{12}$$

The dimensionless governing equations are

$$\tilde{\boldsymbol{u}}_{1t} + (\tilde{\boldsymbol{u}}_1\cdot\nabla)\tilde{\boldsymbol{u}}_1 = \\ = -\nabla\tilde{p}_1 + \tilde{\mu}\Delta\tilde{\boldsymbol{u}}_1 - \tilde{g}\boldsymbol{j}, \tag{13}$$

$$\tilde{\boldsymbol{u}}_{2t} + (\tilde{\boldsymbol{u}}_2\cdot\nabla)\tilde{\boldsymbol{u}}_2 = \\ = -r\nabla\tilde{p}_2 + m\tilde{\mu}r\Delta\tilde{\boldsymbol{u}}_2 - \tilde{g}\boldsymbol{j}, \tag{14}$$

$$\nabla\cdot\tilde{\boldsymbol{u}}_{1,2} = 0, \tag{15}$$

while the corresponding boundary conditions at the walls are now

$$\tilde{\boldsymbol{u}}_1 = 0, \bar{V}_1 = 0 \text{ at } y = -1/2, \tag{16}$$

$$\tilde{\boldsymbol{u}}_2 = 0, \bar{V}_2 = \bar{V} \text{ at } y = +1/2, \tag{17}$$

with $\bar{V} = \bar{V}^*/V^*$. Interfacial boundary conditions (4)-(9) and the stress tensor (10) are also transformed in a straightforward manner.

2.2. Linear Stability Theory

In the present subsection we consider linear perturbations about the base state solution, described by a flat interface, zero velocities and a uniform electric field. There is also an electrically induced pressure difference across the interface

$$p_E = p_2 - p_1 = \frac{2\bar{V}^2}{(\epsilon+1)^2}(\epsilon_1 - \epsilon_2\epsilon^2),$$

and this is accounted for in the theory. We linearise with respect to $\delta \ll 1$:

$$\tilde{\boldsymbol{u}}_{1,2} = \delta\hat{\boldsymbol{u}}_{1,2}, \tilde{S} = \delta\hat{S}, \\ \tilde{p}_1 = -\tilde{g}y + \delta\hat{p}_1, \; \tilde{p}_2 = -\frac{\tilde{g}y}{r} + p_E + \delta\hat{p}_2, \\ \tilde{V}_1 = \frac{\bar{V}}{\epsilon+1}(2y+1) + \delta\hat{V}_1, \\ \tilde{V}_2 = \frac{\bar{V}}{\epsilon+1}(2\epsilon y+1) + \delta\hat{V}_2,$$

and assume normal mode solutions of the form

$$\hat{\boldsymbol{u}}_{1,2}(x,y,t) = \breve{\boldsymbol{u}}_{1,2}(y)e^{ikx+\omega t} + c.c., \\ \hat{V}_{1,2}(x,y,t) = \breve{V}_{1,2}(y)e^{ikx+\omega t} + c.c., \\ \hat{p}_{1,2}(x,y,t) = \breve{p}_{1,2}(y)e^{ikx+\omega t} + c.c., \\ \hat{S}(x,t) = \breve{S}e^{ikx+\omega t} + c.c.,$$

where $c.c.$ is the notation used for complex conjugates. With the appropriate boundary conditions, the eigenfunctions are determined in closed form. The interfacial and boundary conditions then give rise to a system of homogeneous linear equations for the unknown constants appearing in the eigenfunctions. With given parameters (densities, viscosities, permittivities, electric potential difference etc.) we derive a transcendental eigenrelation for the growth rate $\omega(k)$, which is calculated numerically.

In order to validate the theory, we use direct numerical simulations performed in Gerris (Popinet, 2003), described in more detail in section 3. The initial interfacial shape is given by $S(x,0) = A_i\cos(2\pi qx)$, where $q \geq 1$ is used to manipulate the wavenumber of the perturbation and $A_i = \mathcal{O}(10^{-3})$ is the initial amplitude. An example computation for

$r = 6, m = 0.1, \epsilon = 2, \tilde{\mu} = 0.025, \tilde{\sigma} = 0.1$ and voltage potential differences $\bar{V}$ varying from 2.0 to 5.0 is shown in Fig. 2. Excellent agreement is found between theoretical predictions and numerical results (an extended version of this analysis is shown in Cimpeanu and Papageorgiou (2014)). An increase in the imposed voltage potential difference translates to a larger band of instability and higher growth rates. These findings encourage us to direct our efforts towards practical problems in microfluidic mixing (section 3) and pumping phenomena (section 4).

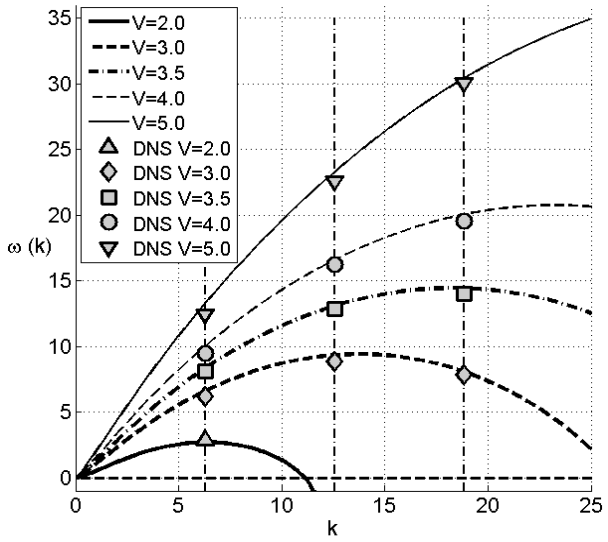

Fig. 2. Example dispersion relation curve computation, for various values of voltage potential difference $\bar{V}$. Curves originate from theoretical stability computations, while symbols are deduced from direct numerical simulations.

3. Microfluidic Mixing

Our aim is to model efficient control procedures in small scale geometries, where physical experiments are often difficult to construct, manipulate and analyse. The presented stability theory allows us to identify the most unstable wavenumbers in relevant flows and we use this information to tailor electric field protocols for enhanced mixing.

For the numerical experiments we use Gerris (Popinet, 2003; Lopez-Herrera et al., 2011), a volume-of-fluid package with tremendous capabilities. Mesh adaptivity, accurate multiphase fluid representation, parallelisation and multi-physics features are just a few of the reasons why the package is an ideal choice for our study.

One of the simplest ways to initiate interfacial motion in the fluid-fluid systems considered here is a sequence of on and off positions of the electric field. The instability caused during the on-times produces dynamics that enhance mixing. We switch the electric field off before interfacial touchdown occurs on the walls (beyond the scope of the present work) and allow the interface to retreat close to its initial position. We repeat this procedure to sustain oscillations in the flow that greatly improve mixing effects in small scale geometries. Furthermore, the proposed on-off protocols are easy to design from a practical perspective.

Despite the fact that the proposed control mechanism involves a time-dependent electric field, the induced magnetic field is negligible (estimated to be of $\mathcal{O}(10^{-10})$ Teslas or less) due to the length scales involved. Secondly, with a period of oscillation of $\mathcal{O}(10^{-2})$ s or more, the frequency is of at most $\mathcal{O}(10^{2})$ Hz, well below the kHz range where the electrostatic approximation still holds. Fig. 3 describes a series of six on-off protocols, where the horizontal axis represents dimensionless time. The shaded regions in each of the plots illustrate the time intervals when the electric field is turned on and the flow is subjected to a vertical electric field. For this set of experiments we use $r = 6, m = 0.25, \epsilon = 2, \tilde{\mu} = 0.1, \tilde{\sigma} = 0.5$ and a voltage potential difference $\bar{V}$ of 15.0. The parameters correspond to a system of size $L = 1.9$ mm, for a duration of roughly 0.3 s in total. Fluid 1 has properties representative of a typical oil (olive oil has been selected), while the ratios in density, viscosity and permittivity of $\mathcal{O}(1)$ pertain to a wide range of choices for the second fluid. A strong contrast in density is preferred from the computational standpoint due to the faster relaxation time of the interface position during the intervals when the electric field is switched off. A droplet of dimensionless radius $r = 0.15$ is constructed in the upper fluid within our computational domain (Fig. 1). The droplet carries the same properties as the upper

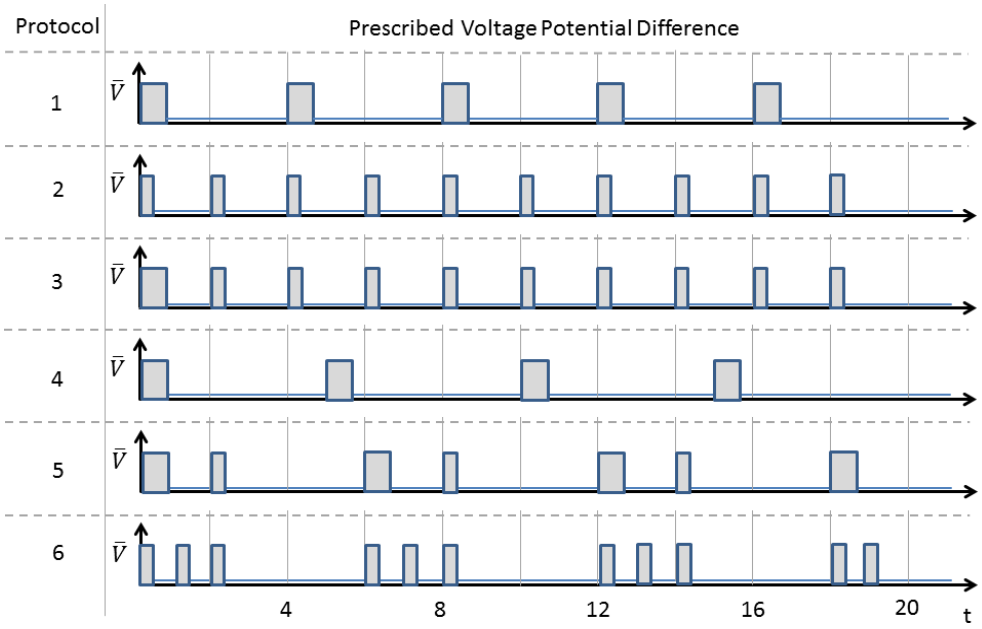

Fig. 3 Six imposed on-off protocols, where shaded regions represent the times when the electric field is kept on with a constant voltage, enabling the destabilisation of the fluid-fluid interface.

fluid, replicating the effect of a dye of different colour. By observing the concentration field c of this passive tracer in time, we deduce the level of mixing induced by the action of the electric field. Sample evolutions of the passive tracer field are produced in Table 1, where protocols 3 and 5 are shown at different times of the simulation.

There are various ways to quantify the degree of mixing (Glasgow et al., 2003; Lu et al., 2002). We chose the statistical expression of Jha et al. (2011), where a mixing index $\chi(t)$ is defined as $\chi(t) = 1 - \beta^2(t)/\beta^2_{max}$, with $\beta^2 \equiv \langle c^2 \rangle - \langle c \rangle^2$. Brackets $\langle \cdot \rangle$ stand for spatial averaging over our dynamic domain. β^2_{max} is the variance for the fully segregated state. $\chi = 1$ then translates to a perfectly mixed system, while $\chi = 0$ depicts a completely segregated environment. Using this type of measurement, Fig. 4 shows the dynamics of the mixing index in time for each of the six constructed protocols. Efficient mixing usually occurs when a strong destabilizing electric field persists for a moderate amount of time, such that the active interface is close to reaching the channel walls. After this spread has occurred, successive on-off switches of short duration will sustain interfacial oscillations and lead to highly efficient mixing, with indexes exceeding 0.7, which are very competitive against other forms of induced mixing.

We note that numerical artifacts in the passive tracer advection lead to minor breaches through the interface (observable in Table 1); a careful study reveals that this does not affect the calculated degree of mixing (the amount of dyed fluid outside the desired region is negligible and this numerical process is restricted to the passive tracer, computed by approximating the velocity field). Furthermore, stringent error tolerances and increased grid refinement levels can be imposed to completely eliminate such effects.

The level of improvement in mixing is also quantified in the light of comparing results to molecular diffusion. Using Fick's law in two dimensions, the radius of diffusion of particles is described by $x^2 \sim 4Dt$, where D is the self-diffusion coefficient inside a given fluid, which ranges within $\mathcal{O}(10^{-12} - 10^{-9})$ for fluids of interest such as oil and water (Denkova et al., 2004; Holz et al., 2000). Measuring the spread via molecular diffusion within a fluid with self-diffusion coefficient of $D = 10^{-11}$, we notice that it is no larger than $3.5 \cdot 10^{-6}$ m in the time frame of the numerical experiments in the $1.9 \cdot 10^{-3}$ m

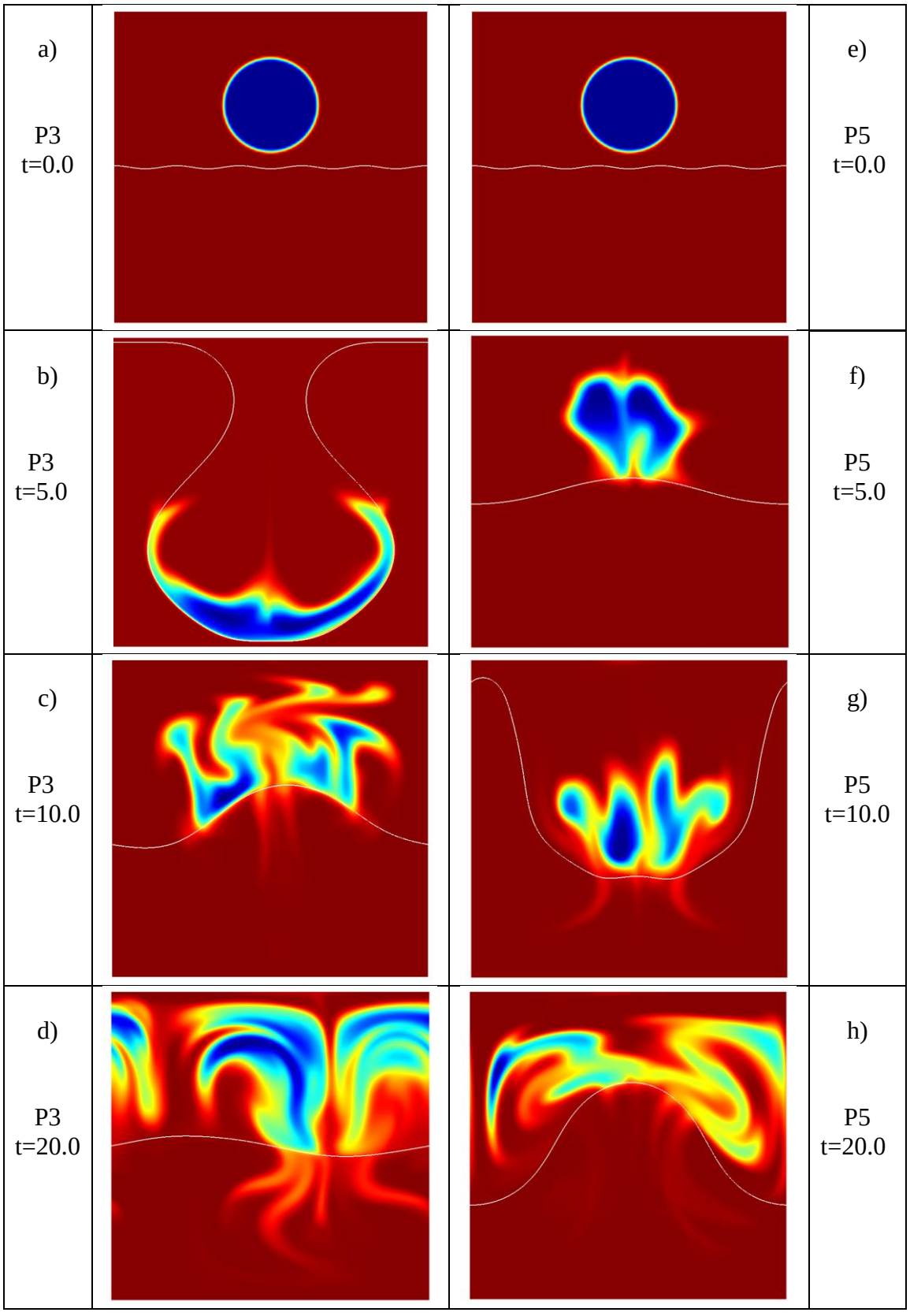

Table 1. The passive tracer field and active fluid-fluid interface highlighted in white under the action of protocol 3 (left) and protocol 5 (right) at four different time steps: t=0.0 (top row), t=5.0, t=10.0 and t=20.0 (bottom row). The succession of plots shows the gradual mixing of the passive tracer under the action of the electric field.

channel, which is several orders of magnitude less than the displacement of particles under the action of electrohydrodynamic control. The evolution of the mixing index solely via molecular diffusion has been computed for reference (see Fig. 4) and evolves from 0.0369, the starting value given by the discretisation of the concentration field, to 0.0377 by the end of the numerical experiments. Therefore the action of the imposed electric field protocols produces a striking impact in the dynamics of the flow.

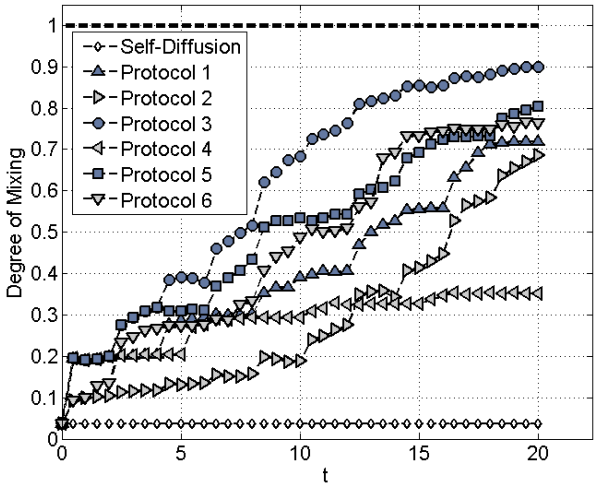

Fig. 4. Evolution of mixing index $\chi(t)$ under the action of electrohydrodynamic control.

4. Induced Pumping

We use a similar type of analysis to model pumping in microgeometries. Instead of a uniform electric field, we consider a spatiotemporally varying voltage on one of the electrodes (taking care that the electrostatic approximation is still valid within the range of physically relevant frequencies). Such a model can be constructed in the form of a travelling disturbance, which replicates the structure of a sequence of parallel strip electrodes on a substrate, switched on and off in successive order. The reader is referred to Cimpeanu and Papageorgiou (2014) for a more detailed insight in this direction. We use such a rationale for the bottom electrode and consider a boundary condition of the form $V_1(x,-1/2\,,t)=\bar{V}(t)$, given by

$$\bar{V}(t)=C+\frac{2A_r}{\pi}\left[\tan^{-1}\left(\frac{x-x_L-U_rt}{\delta'}\right)-\right.$$
$$\left.-\tan^{-1}\left(\frac{x-x_R-U_rt}{\delta'}\right)\right].$$

The boundary condition produces a uniform voltage of magnitude C, with a superimposed hump of magnitude A_r, travelling with velocity U_r in a prescribed direction. The size of the transition region from C to $C+A_r$ is of order $\delta'=10^{-3}$. We can add several such humps in order to match the structure of the most unstable wavenumber with given parameters of the flow. The pumping is induced by first switching on a uniform electric field of magnitude C, such that the most unstable wavenumber is excited and grows until the interface is in close vicinity of the channel walls. The time-dependent voltage is then prescribed and a voltage travelling wave forms at the boundary. The flow field is steered into a desired direction and the procedure can be optimised by tuning parameters A_r and U_r.

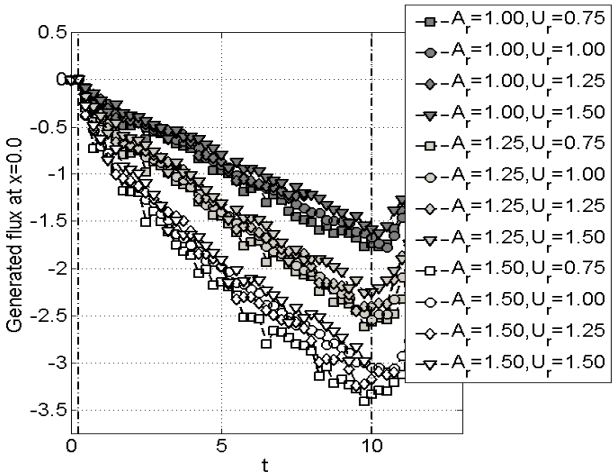

Fig. 5. Flux evolution for different amplitudes and velocities of the travelling wave voltage distribution in 12 different configurations.

We design 12 direct numerical simulations, with chosen values $A_r \in \{1.0,1.25,1.5\}, U_r \in \{0.75,1.0,1.25,1.5\}$. The reasoning behind these values is the following. If the amplitude of the hump is too small, the effect of the travelling wave is not transmitted to the flow and interfacial wall touchdown occurs. On the other hand, prescribing strong amplitudes may produce interfacial rupture (droplet formation) and cause unwanted phenomena in the flow. Velocity U_r is only limited by physical (experimental) constraints.

We quantify the success of the method by examining the flux in the

microchannel at $x = 0.0$ by

$$F_0(t) = \int_{-0.5}^{+0.5} u(0, y, t)dy.$$

The results are described in Fig. 5, where during the period of the spatiotemporally varying voltage (between $t = 0.25$ and $t = 10.0$), the flow exhibits leftward movement in a manner that is directly proportional to the amplitude A_r, while the velocity U_r plays a secondary role. An extensive analysis of the flow, including the evolution of the fluid velocity fields during the period of the spatiotemporally varying voltage, is provided by Cimpeanu and Papageorgiou (2014). We note a possible extension to a similar construction on the top electrode, to be calibrated with an adjusted phase.

5. Conclusion

The methods described in the present study have been proven successful in the context of electrohydrodynamic control in microchannels. We have identified powerful mixing mechanisms, as well as a technique to induce pumping at small scales without the necessity of moving parts or imposed velocity fields. Driven solely by electric field dynamics, the interfacial behaviour can be customised for typical industrial applications and further optimised for added efficiency.

Acknowledgements

D.T.P. acknowledges the support of EPSRC under grant EP/K041134/1, while R.C. gratefully acknowledges a Roth Doctoral Fellowship from the Department of Mathematics, Imperial College London.

References

Cimpeanu, R., Papageorgiou, D.T., Petropoulos, P.G., 2014. On the control and suppression of the Rayleigh-Taylor instability using electric fields. Phys. Fluids 26, 022105.

Cimpeanu, R., Papageorgiou, D.T., 2014. On the Generation of Nonlinear Travelling Waves in Confined Geometries Using Electric Fields. Phil. Trans. Royal Society A 28, vol. 372, 2020, 20140066.

Denkova, P.S., Tcholakova, S., Denkov, N.D., Danov, K.D., Campbell, B., Shawl, C., Kim, D., 2004. Evaluation of the Precision of Drop-Size Determination in Oil/Water Emulsions by Low-Resolution NMR Spectroscopy. Langmuir 20, 11402-11413.

El Moctar, A.O., Aubry, N., Batton, J., 2003. Electrohydrodynamic microfluidic mixer. Lab Chip 3, 273-280.

Glasgow, I., Aubry, N., 2003. Enhancement of microfluidic mixing using time pulsing. Lab Chip 3, 114-120.

Goullet, A., Glasgow, I., Aubry, N., 2005. Dynamics of microfluidic mixing using time pulsing. Discrete and Continuous Dynamical Systems Suppl. Vol., 327-336.

Holz, M., Heil, S.R., Sacco, A., 2000. Temperature-dependent self-diffusion coeff. of water and six selected molecular liquids for calibration in accurate ^{1}H NMR PFG measurements, PCCP 2, 4740-4742.

Jha, B., Cueto-Felgueroso, L., Juanes, R., 2011. Fluid Mixing from Viscous Fingering. Phys. Rev. Letters 106, 194502.

Lee, C.-Y., Chang, C.-L., Wang, Y.-N., Fu, L.-M., 2011. Microfluidic mixing: A review. Int. J. Mol. Sci. 12, 3263-3287.

Lopez-Herrera, J.M., Popinet, S., Herrada, M.A., 2011. A charge-conservative approach for simulating electro hydrodynamic two-phase flows using volume-of-fluid. J. Comp. Phys. 230, 1939.

Lu, L.-H., Ryu, K.S., Liu, C., 2002. A magnetic mirostirrer and array for microfluidic mixing. Journal of Microelectromech. Systems 11, 462-469.

Melcher, J.R., 1961. Electrohydrodynamic and magentohydrodynamic surface waves and instability. Phys. Fluids 4, 1348.

Ozen, O., Aubry, N., Papageorgiou, D.T., Petropoulos, P.G., 2006. Electrohydrodynamic linear stability of two immiscible fluids in channel flow. Electrochimica Acta 51, 5316-5323.

Ozen, O., Aubry, N., Papageorgiou, D.T., Petropoulos, P.G., 2007.Linear stability of a two-fluid interface for electrohydrodynamic mixing in a channel. J. Fluid Mech. 583, 347-377.

Popinet, S., 2003. Gerris: A tree-based adaptive solver for the incompressible Euler equations in complex geometries. J. Comp. Phys. 190, 572.

Saville, D.A., 1997. Electrohydrodynamics: The Taylor-Melcher leaky dielectric model. Annu. Rev. Fluid Mech. 29, 27.

Taylor, G.I., McEwan, A.D., 1966. The stability of a horizontal fluid interface in a vertical electric field. J. Fluid Mech. 22, 1.